

On the distribution of ozone in stratospheric anticyclones

V. L. Harvey,¹ R. B. Pierce,² M. H. Hitchman,³ C. E. Randall,¹ and T. D. Fairlie²

Received 6 May 2004; revised 31 August 2004; accepted 20 September 2004; published 24 December 2004.

[1] Twelve years (1991–2003) of satellite occultation ozone data are combined with a climatology of stratospheric anticyclones and polar vortices to quantify the climatological ozone differences between air mass types. Ozone data from the Stratospheric Aerosol and Gas Experiment (SAGE) II, the Halogen Occultation Experiment (HALOE), the Polar Ozone and Aerosol Measurement (POAM) II and III missions, and the Improved Limb Atmospheric Spectrometer (ILAS) sensor are used in this study. Daily ozone measurements in the 400–1600 K altitude range are categorized as being either (1) in an anticyclone, (2) in a polar vortex, or (3) in neither (hereinafter referred to as “ambient”). Monthly mean ozone is then calculated in each air mass category from data combined over all years. This study focuses on ozone differences between anticyclones and the ambient environment. A composite annual cycle of ozone in ambient regions is compared to ozone in anticyclones as a function of altitude and latitude. Ozone differences result from both anomalous transport and photochemistry in the vicinity of stratospheric anticyclones. The relative importance of transport versus chemistry is inferred from the long-term ozone anomalies observed here. In summer, ozone gradients between different air mass types are small. In other seasons, results indicate three distinct vertical regimes at high latitudes. Below ≈ 600 K, anticyclones coincide with regions where ozone is reduced by 10–50% during the winter. Between 600 and 900 K from fall to midwinter, anticyclones are associated with $\approx 10\%$ more ozone than ambient air masses. Positive ozone anomalies are also observed in low-latitude anticyclones within this vertical layer; however, they are half the size of their high-latitude counterparts and peak several months later. Above 900 K the abundance of ozone in anticyclones is $\approx 10\%$ less than in the surrounding air. This upper stratospheric regime results from the formation of “low-ozone pockets” (LOPs) in stratospheric anticyclones. All LOPs that formed between November 1991 and November 2003 and were observed by a satellite used in this study (108 pockets) are documented here in the most comprehensive catalog of LOPs to date.

INDEX TERMS: 0341 Atmospheric Composition and Structure: Middle atmosphere—constituent transport and chemistry (3334); 3309 Meteorology and Atmospheric Dynamics: Climatology (1620); 3334 Meteorology and Atmospheric Dynamics: Middle atmosphere dynamics (0341, 0342); *KEYWORDS:* tracer transport, ozone, stratosphere

Citation: Harvey, V. L., R. B. Pierce, M. H. Hitchman, C. E. Randall, and T. D. Fairlie (2004), On the distribution of ozone in stratospheric anticyclones, *J. Geophys. Res.*, 109, D24308, doi:10.1029/2004JD004992.

1. Introduction

[2] Air masses are large bodies of air that have distinct kinematic, thermodynamic, or chemical characteristics. They form where air stagnates or is sequestered long enough through dynamical constraints to acquire a signature representative of the local radiative environment. In the stratosphere, the wintertime polar vortices are known to isolate air to a degree that is sufficient to form air masses

within them. These “vortex air masses” are recognized as regions surrounded by large horizontal gradients of potential vorticity (PV) and trace species [e.g., Proffitt *et al.*, 1989; Lahoz *et al.*, 1993; Waugh, 1997]. Especially clear observations of the distinct chemical characteristics of vortex air masses are provided when vertical profiles of trace species intersect the vortex edge [Kreher *et al.*, 1999; Manney *et al.*, 2000]. Previous studies have demonstrated the usefulness of first categorizing tracer data based on whether the sample is currently, or had recently been, located inside the vortex [e.g., Kent *et al.*, 1985; Pierce *et al.*, 1994; Abrams *et al.*, 1996; Newman *et al.*, 1996; Michelsen *et al.*, 1998, 1999; Choi *et al.*, 2002].

[3] Air masses also originate in a region referred to as the tropical stratospheric reservoir (TSR), the base of which is estimated to be several kilometers above the tropical tropopause [Trepte and Hitchman, 1992]. Large meridional

¹Laboratory for Atmospheric and Space Physics, University of Colorado, Boulder, Colorado, USA.

²NASA Langley Research Center, Hampton, Virginia, USA.

³Department of Atmospheric and Oceanic Sciences, University of Wisconsin, Madison, Wisconsin, USA.

gradients in trace species suggest this region extends upward to at least the stratopause [e.g., *Randel et al.*, 1993]. The width of the TSR ranges from approximately 20°S to 20°N; however, the instantaneous location of TSR boundaries varies with longitude, altitude, season, and phase of the quasi-biennial oscillation (QBO) [*Grant et al.*, 1996]. Between the tropopause and the TSR (in and above the tropical tropopause layer, or TTL [*Gettelman and de Forster*, 2002]) air flows poleward following the upward branch of the Hadley circulation. Above ≈600 K, however, transport out of the TSR occurs intermittently and predominantly into the winter hemisphere [*Trepte et al.*, 1993; *Hitchman et al.*, 1994; *Chen et al.*, 1994; *Plumb*, 2002]. Air enters the TSR from the tropical upper troposphere and then may stay confined to tropical latitudes for many months. Observations of stratospheric aerosol as well as contour advection calculations estimate only 5–10% of the mass between 20°S and 20°N is transported poleward out of the TSR each month [*Grant et al.*, 1996; *Waugh*, 1996]. During individual transport events “tongues” appear in tracer distributions that extend eastward out of the tropics into midlatitudes [e.g., *Leovy et al.*, 1985]. These dramatic events require midlatitude westerlies at lower altitudes to permit tropospheric disturbances to propagate upward [*Waugh*, 1996]. The timing of such events has been linked to the equatorward displacement of the polar night jet [*Waugh*, 1993]. In fact, tongues rich in tropical tracers form near the jet entrance region and the western flank of developing anticyclones [*Leovy et al.*, 1985]. These high-pressure systems originate in low latitudes, travel poleward and eastward around the vortex, and transport low PV air that is dry but rich in ozone, methane, nitrous oxide, and aerosol to higher latitudes [*Rood et al.*, 1992; *Randel et al.*, 1993; *Waugh*, 1993; *O’Neill et al.*, 1994; *Ruth et al.*, 1994; *Chen et al.*, 1994; *Yang*, 1995; *Polvani et al.*, 1995; *Manney et al.*, 1993, 1995a, 1995b, 1998; *Lahoz et al.*, 1994, 1996; *Harvey et al.*, 1999; *Riese et al.*, 2002]. These observations provide the motivation for this work, which is to determine whether the culmination of repeated transport events leaves a climatological ozone signature in stratospheric anticyclones. If this is the case, anticyclone frequency may be a useful proxy to estimate the dynamical contribution to ozone variability.

[4] Both dynamical and chemical processes affect the budget of ozone in the stratosphere, with the relative contributions depending on altitude, latitude, and season. Below about 25 km, ozone is dynamically controlled throughout the year [*Garcia and Solomon*, 1985]. Dynamical processes also control ozone distributions throughout the stratosphere in the polar night [*Garcia and Solomon*, 1985; *Dougllass and Rood*, 1986; *Kulikov et al.*, 2002]. The transition from dynamical to photochemical control shifts gradually downward from the upper stratosphere as the sun returns to the polar region. At high latitudes, the summertime transition between photochemical and dynamical control occurs near 25 km [*Garcia and Solomon*, 1985; *Perliski and London*, 1989; *Randall et al.*, 1995]. At low latitudes and midlatitudes, photochemical control is dominant throughout the year in the middle and upper stratosphere [*Garcia and Solomon*, 1985]. In the upper stratosphere the distribution of ozone is controlled photochemically and many studies have established its negative correlation with temperature [e.g., *Finger et al.*, 1995; *Ward*

et al., 2000]. The photochemically controlled ozone budget is determined by a balance between production in the tropical source region ($O_2 + O$), and catalytic loss processes. Throughout most of the altitudes of interest here (from about 24 to 40 km), the NO_x catalytic cycle is the dominant loss mechanism; in the lower stratosphere, the halogen (Cl, Br) and HO_x catalytic cycles are more important [*Lary*, 1997]. The trade-offs between dynamical and chemical processes lead to a general picture of decreasing (increasing) ozone with increasing latitude throughout the stratosphere above (below) about 20 km [e.g., *Rasch et al.*, 1995].

[5] Dynamics and chemistry are particularly coupled during the formation of “low-ozone pockets” (LOPs) in stratospheric anticyclones [*Manney et al.*, 1995c, 2001]. The mechanism responsible for the formation of LOPs is to confine air at high solar zenith angles long enough for ozone to relax toward local photochemical equilibrium [*Morris et al.*, 1998; *Nair et al.*, 1998]. While such isolation within the Aleutian High in the Northern Hemisphere (NH) has been demonstrated [e.g., *Seo and Bowman*, 2000], it is not known how often sufficient isolation is achieved and maintained. Thus the net contribution anticyclones make in redistributing ozone remains unquantified. One of the goals of this study is to provide such an estimate by separating ozone measurements that are inside anticyclones (and polar vortices) from those that are not. When anticyclones develop an interior LOP, this mitigates the signature that high-ozone anticyclones acquire during poleward transport events [*Calisesi et al.*, 2001]. Climatological ozone differences between anticyclones and ambient regions assess the net effect of these two competing processes and when and where each one is dominant. This work is similar in spirit to that of *Harvey et al.* [1999] with a focus on ozone rather than aerosol. However, a more physical approach is used here in the separation of measurements. Instead of simply binning ozone in longitude or within a predetermined region, data are gathered based on whether they are contained within the discrete spatial extent of an anticyclone [*Harvey et al.*, 2002]. The resulting ozone distributions are then calculated within each air mass type and are compared. Hereafter, ozone “anomalies” refer to the difference between the ozone concentration in an anticyclone and the ambient environment. A positive anomaly implies higher ozone in the anticyclone.

[6] Section 2 discusses the data and analysis methods used in this study. Particular attention is given to differences between satellite sampling patterns. In section 3, the ozone climatology is presented. Monthly mean ozone differences between anticyclones and ambient air are averaged over the 1991–2003 time period and shown as a function of latitude, altitude and time of the year. Section 4 documents LOPs that occurred between November 1991 and November 2003 and were observed by one or more of the satellites used here. Section 5 summarizes the results.

2. Data and Analysis Methods

[7] Met Office (MetO) global analyses of temperature, geopotential height, and winds from 11 November 1991 through November 2003 are used in this study [*Swinbank and O’Neill*, 1994]. The MetO data set used here was originally produced in support of the Upper Atmosphere

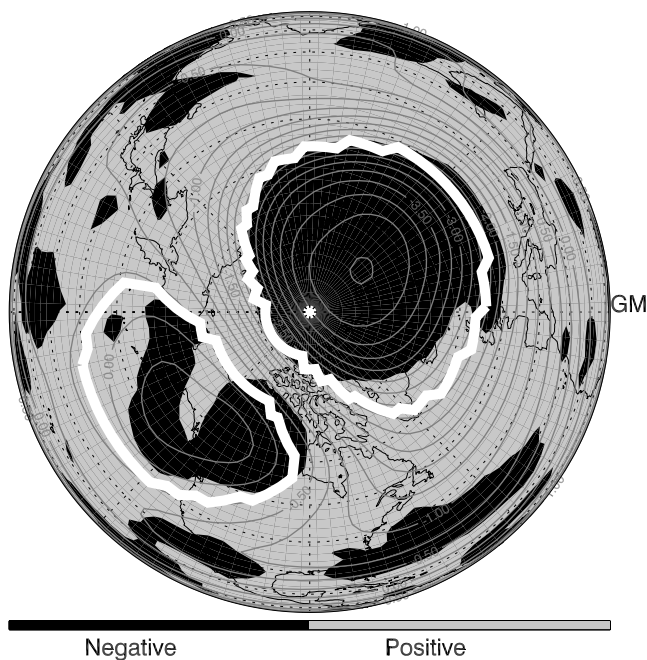


Figure 1. Northern Hemisphere polar stereographic projection of the stream function (contour interval is 2.5×10^{-7}) and Q fields (shaded) on 18 December 2003 at 1000 K. Thick white contours represent the edges of the Arctic vortex (over the pole) and Aleutian High (over the North Pacific). The Greenwich Meridian points to the right.

Research Satellite (UARS) project and is available once daily (12Z) dating back to 17 October 1991. Mid-November 2000 and late October 2003 mark major changes in the MetO analyses with the former involving the implementation of 3-D variational assimilation [Lorenc *et al.*, 2000] and the latter a “New Dynamics” version of the Unified Model. Analyzed fields in the troposphere and lower stratosphere are similar to those from the previous system; however, the stratopause is about 10 K warmer than in the prior version, with the lower mesosphere cooler than before. Time series of anticyclone frequency in the upper stratosphere do not show discontinuities in late 2000 or 2003, lending confidence that our results are robust to these changes. A comparison of results using different analyses and incorporating additional ozone data sets will be performed at a later date.

[8] The spatial resolution is 2.5° latitude by 3.75° longitude on the following 22 pressure levels: 1000 hPa to 0.316 hPa in increments of $1000 \times 10^{-i/6}$, where $i = 0$ to 21. The data are linearly interpolated from isobaric to the following potential temperature surfaces: 400–550 K by 25 K, 600 to 1000 by 100 K, and 1000 to 1600 by 200 K. From 400–550 K the vertical resolution is ≈ 1 km. From 550–1600 K there are 2–3 km between potential temperature surfaces. Hereafter, potential temperature is used as the vertical coordinate.

[9] The following briefly explains the method with which anticyclones and the polar vortices are identified at each altitude on each day. For a detailed discussion of the algorithms and anticyclone/polar vortex frequency distributions see Harvey *et al.* [2002]. The velocity field is

decomposed into rotational and divergent components from which the stream function (ψ) field is used to characterize the large-scale flow. The scalar quantity, Q , is also calculated to provide a measure of the relative contribution of strain and rotation in the flow [Haynes, 1990; Fairlie, 1995]. It is derived by separating the velocity gradient tensor, \mathbf{L} , into the rate of deformation tensor, $\mathbf{D} = \frac{1}{2}(\mathbf{L} + \mathbf{L}')$, and the solid body spin tensor, $\mathbf{W} = \frac{1}{2}(\mathbf{L} - \mathbf{L}')$ [see Malvern, 1969]. In tensor notation, $2Q = \mathbf{D} : \mathbf{D} - \mathbf{W} : \mathbf{W}$ where the operator “:” represents the tensor scalar product. Neglecting the vertical shear component, Q is given in spherical coordinates by

$$Q = \frac{1}{2} \left(\frac{1}{a \cos \phi} \frac{du}{d\lambda} - \frac{v}{a} \tan \phi \right)^2 + \frac{1}{2} \left(\frac{1}{a} \frac{dv}{d\phi} \right)^2 + \left(\frac{1}{a^2 \cos \phi} \frac{du}{d\phi} \frac{dv}{d\lambda} + \frac{u \tan \phi}{a^2} \frac{du}{d\phi} \right)$$

where ϕ = latitude, λ = longitude, u = zonal wind, v = meridional wind, and a = the radius of the Earth. The first two terms on the left-hand side are the shear terms and are always positive while the last term is the rotation and is always negative. Thus Q is positive (negative) where strain (rotation) dominates the flow. This quantity is used to delineate the spatial extent of stable circulation systems.

[10] Figure 1 illustrates the separation of the stratosphere into distinctly different air masses. Shown is a NH orthographic projection on 18 December 2003 at 1000 K of Q (shaded) and ψ (contours). The Arctic vortex encircles the North Pole while the Aleutian High is over the North Pacific. The thick white contours represent the edges of vortices identified at this altitude. Negative Q indicates where rotation is dominant, such as in the Arctic vortex and in the anticyclone. Positive Q is found near the polar night jet where wind shear is large. The “edges” of these closed circulation systems are defined as the ψ contour farthest from the center of rotation with $\int Q dA < 0$, where A is defined as the area enclosed by the ψ isopleth. Area integrated relative vorticity is used to determine the sign of rotation. On each day, a 3-D gridded “marker” field is generated where grid points inside anticyclones (polar vortices) are assigned a value of -1 (1) while grid points in ambient regions are set to 0. A vertical “marker” profile is interpolated in time and space to each satellite ozone measurement and used to identify sampled air mass type as a function of altitude. Monthly mean ozone is then calculated separately for measurements located in anticyclones, in polar vortices, and in ambient regions as a function of latitude and altitude. Ozone anomalies in the polar vortices will be presented elsewhere. In order to remove sampling biases between the ambient and anticyclone categories, we only binned those ambient measurements that were located within 10° latitude of corresponding anticyclone data. This was necessary because there was much more ambient data from a wider range of latitudes than anticyclone data. Composite monthly mean ozone in anticyclones and ambient regions is derived from data binned over multiple years; i.e., a January mean results from all January data combined. Probability distribution functions of relative vorticity in ambient regions are narrow Gaussians centered about zero in most of the winter stratosphere. Below ≈ 450 K, the

Table 1. Satellite Data Characteristics

	SAGE II	HALOE	POAM II	ILAS	POAM III
Platform	ERBS	UARS	SPOT-3	ADEOS	SPOT-4
Lifetime	Oct. 1984 to present	Oct. 1991 to present	Oct. 1993 to Oct. 1996	Oct. 1996 to June 1997	April 1998 to present
Spatial coverage	80°S–80°N	80°S–80°N	63°–88°S, 55°–71°N	64°–73°N	63°–88°S, 55°–71°N
Data version	6.2	19	6	5.2	3
Vertical resolution	~1 km	~2 km	~1–1.5 km	~2–3.5 km	~1 km

distribution broadens as the ambient category contains cutoff cyclones in the upper troposphere/lower stratosphere (UTLS) that are neither identified nor subsequently removed. Circumpolar anticyclones are not identified and thus ozone inside them is not added to the anticyclone category. These anticyclones that encircle the pole are typically mature systems that migrated poleward from lower latitudes [Harvey *et al.*, 2002]. It is likely that LOPs are present in these persistent anticyclones. Thus the effect of omitting these ozone profiles from the anticyclone category acts to dampen the LOP signature in anticyclones and provide a conservative estimate of their effect on the overall ozone distribution.

2.1. Satellite Data

[11] Ozone data from the Stratospheric Aerosol and Gas Experiment (SAGE) II, the Halogen Occultation Experiment (HALOE), the Polar Ozone and Aerosol Measurement (POAM) II and III missions, and the Improved Limb Atmospheric Spectrometer (ILAS) sensor are used in this study. Table 1 lists each instrument's spatial and temporal coverage, vertical resolution, and the data version used here. SAGE II and HALOE measure ozone at a wide range of latitudes that vary throughout the year while POAM and ILAS continuously sample high latitudes. In this study, these data are combined in order to increase coverage and extend the ozone record in time.

[12] Combining measurements from different instruments requires consideration of error estimates and biases. The precision of solar occultation measurements of stratospheric ozone is on the order of 3% [Randall *et al.*, 2003]. In terms of accuracy, comparison studies indicate HALOE ozone is systematically 5% lower than SAGE II [Cunnold *et al.*, 1996] with overall differences of 4–12% [Morris *et al.*, 2002]. POAM II ozone agrees with HALOE and SAGE II to within 5–7% above 22 km. Below 22 km POAM II ozone is up to 20% lower than the other instruments [Rusch *et al.*, 1997]. POAM III ozone is within 5% of SAGE II, HALOE, and ozonesonde measurements except below 13 km where it has a 0.1 ppmv high bias [Randall *et al.*, 2003]. Manney *et al.* [2001] compared SAGE II, HALOE, and POAM II and III ozone data and found differences to be less than 0.5 ppmv ($\approx 5\%$) in the upper stratosphere and ≈ 0.25 ppmv in the lower stratosphere. ILAS ozone is within 10% of HALOE, SAGE II, and POAM III between 20 and 50 km [Sugita *et al.*, 2002]. These data validation and comparison studies provide the justification for combining these data. In most cases, the magnitude of these differences is significantly less than those observed between air mass type. In addition, ozone data with stated error estimates greater than 30% are omitted. For each instrument, this became important in the lowermost stratosphere where 20% (50%) of the ozone data at 400 K (350 K) were

removed. This work focuses on altitudes above 400 K where most error estimates are far less than 30%.

2.2. Satellite Sampling Patterns

[13] At any given time there is sampling by some, but not all, of the occultation instruments in different regions of the globe. The SAGE II and HALOE instruments rapidly sweep across the equator and sample all but the highest latitudes, while ILAS and POAM measurements are confined to the polar regions. The frequency with which different air mass types are sampled in each data set depends, in part, on where the instrument repeatedly takes measurements. This section addresses potential biases attributed to the different sampling patterns. Figure 2 shows the annual cycle of zonal mean anticyclone frequency at 800 K derived from the climatology of Harvey *et al.* [2002]. Each day is a 12-year average. Anticyclone frequency exceeds 1.0 on days when there is more than one high-pressure system at a given latitude. This is common, especially in the fall of either hemisphere when the vortex is pole-centered. The latitude of maximum anticyclone frequency moves meridionally in time in accordance with the growth and decay of the polar vortices (indicated by the thick blue contour) [Harvey *et al.*, 2002]. The Antarctic vortex remains circumpolar during most of its life, effectively delaying the entry of anticyclones to high latitudes until spring. The Arctic vortex,

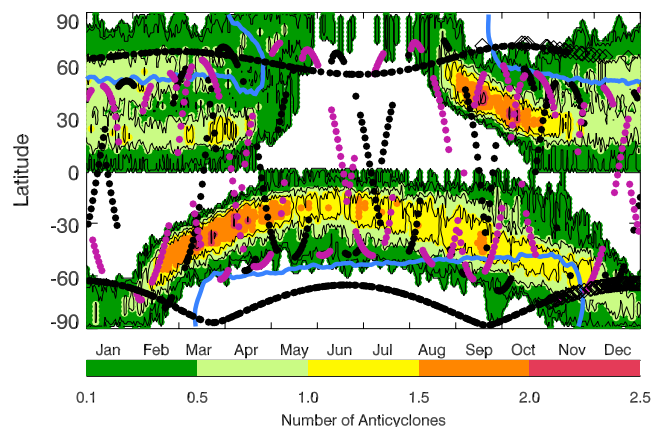


Figure 2. Latitude-time section of the 12-year average annual cycle of anticyclone frequency. Frequencies greater than 1 indicate more than one anticyclone present around a latitude circle. The thick blue contours represent the Arctic and Antarctic vortex edges. The method used to calculate the vortex edge is described by Harvey *et al.* [2002]. Superimposed are the locations of SAGE II (purple circles), HALOE (black circles that sweep across the equator), POAM II (black circles at high latitudes), and ILAS (diamonds) measurements during 1996.

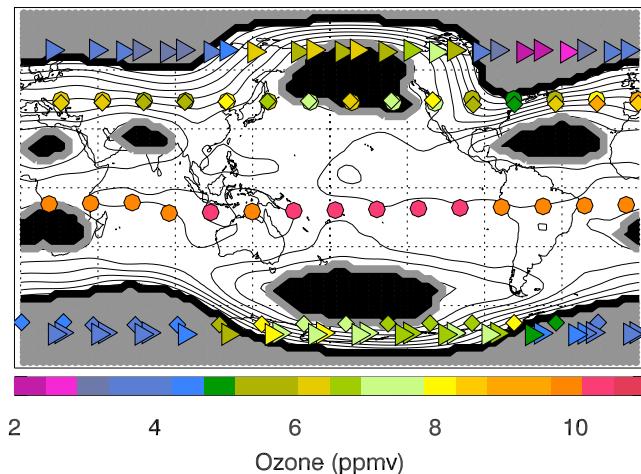


Figure 3. Mercator projection at the 800 K potential temperature surface of the stream function field on 1 November 1996. The Arctic and Antarctic circumpolar vortices are grey with black edges. Anticyclones are black with grey edges. Superimposed are POAM III and ILAS (triangles), SAGE II (diamonds), and HALOE (circles) measurement locations. Each symbol is colored according to the ozone mixing ratio at this altitude.

however, tends to be displaced from the pole during the winter, which allows a single anticyclone, the Aleutian High, to reside poleward of 30°N . This anticyclone is often present near the date line, along with other anticyclones at lower latitudes and different longitudes [Harvey *et al.*, 2002, Figures 6b and 9]. While the summertime anticyclones are identified when not pole-centered, they are not explicitly treated here and results stemming from them are ambiguous at best.

[14] Satellite measurement locations are superimposed over the course of a typical year to illustrate the opportunity for each instrument to sample anticyclones as a function of latitude and time of the year. Both HALOE and SAGE II measure ozone in anticyclones at a wide range of latitudes. The POAM and ILAS instruments routinely provide samples in high-latitude anticyclones in the Arctic. In the Southern Hemisphere (SH) from March through most of October, anticyclones are confined to latitudes too low to be sampled by POAM or ILAS. As a result, these instruments only sample SH anticyclones from mid-October through February. In the absence of POAM and ILAS there is no coverage at high latitudes. Biases introduced by limited sampling are inherently present in the results of this study. The same latitudinal bias is present in both the “ambient” and “anticyclone” ozone, however, and thus cancel out in difference plots between the two. Never the less, these results should not be used to infer trends.

[15] There is considerable day-to-day variability in anticyclone sampling by all instruments because of vortex displacement and elongation as well as the location and size of anticyclones. Figure 3 is a Mercator projection of the stream function field at 800 K on 1 November 1996. The Arctic and Antarctic vortices are present over their respective pole on this day and are shaded grey with a black edge. Anticyclones are shaded black with a grey

edge. The Aleutian High is situated near the date line and 60°N while its counterpart, the Australian High, mirrors it in the Antarctic. POAM II and ILAS (triangles), HALOE (circles), and SAGE II (diamonds) measurement locations are overlaid and colored according to the ozone mixing ratio. On this day, POAM II and ILAS sample in both the Arctic and Antarctic vortices as well as in the Aleutian High. Likewise, both SAGE II and HALOE take measurements in the Aleutian High and in the Antarctic vortex. The Australian High is sampled by SAGE II and an anticyclone over South Africa is observed by HALOE. Anticyclones over North Africa, India, and the Atlantic Ocean are not sampled on this day. All instruments sample in ambient regions.

[16] Overall, $\approx 75\%$ of all SAGE II and HALOE data are located in ambient regions. Of the remaining 25%, 20% are in polar vortices and 5% are in anticyclones. The frequency with which POAM and ILAS sample air masses differs from SAGE and HALOE. Namely, 35% are ambient, 63% are in a polar vortex, and 2% are in anticyclones. Separate climatologies were constructed for SAGE plus HALOE and for POAM plus ILAS to investigate the effect of blending data from different geographic regions. Notable differences will be discussed in the next section. In terms of population densities, over 12 years of combined occultation data yield $\approx 10^4$ ambient measurements in each monthly altitude bin in each hemisphere. However, excluding ambient data that are greater than 10° latitude from corresponding anticyclone data decreases this number by a factor of 10. The number of data points in polar vortices (anticyclones) ranges from 1000 to 5000 (100 to 1500). These large population densities give confidence that our results are statistically significant. In order to ensure that anticyclone sampling is representative, a minimum number of data points from which the means are calculated is set to 50. This is equivalent to about one sample per week over the 12-year period. Months with less than 50 total samples occur less than 7% of the time and are confined to the summer. Roughly 25–50% of all anticyclones, as defined by Harvey *et al.* [2002], are observed by an occultation instrument. Of the anticyclones that are in fact sampled, 10–20% are sampled more than once. Less than 1% of anticyclones are sampled 5 or more times. The most number of samples in a single anticyclone was 18, which occurred 8 times.

3. Climatology of Ozone in Anticyclones

[17] Figure 4 summarizes the climatology of ozone in NH anticyclones. In order to take the latitudinal ozone gradient into consideration and to attempt to further distinguish chemical from dynamical processes, anticyclones are separated into two latitude groups divided at 30°N . It is the latitude of the ozone profile, not of the anticyclone, that determines the latitude bin (i.e., a single anticyclone spanning 30°N could provide ozone data to both the high- and low-latitude bins if there were ozone profiles inside the anticyclone and on both sides of 30°N). This is not a clean separation but illustrates how the relative abundance of ozone in anticyclones is latitude-dependent. Figure 4a shows the 12-year composite annual cycle of ozone in ambient regions between the equator and 30°N as a function of altitude. Mean ozone in ambient air masses is similar to a

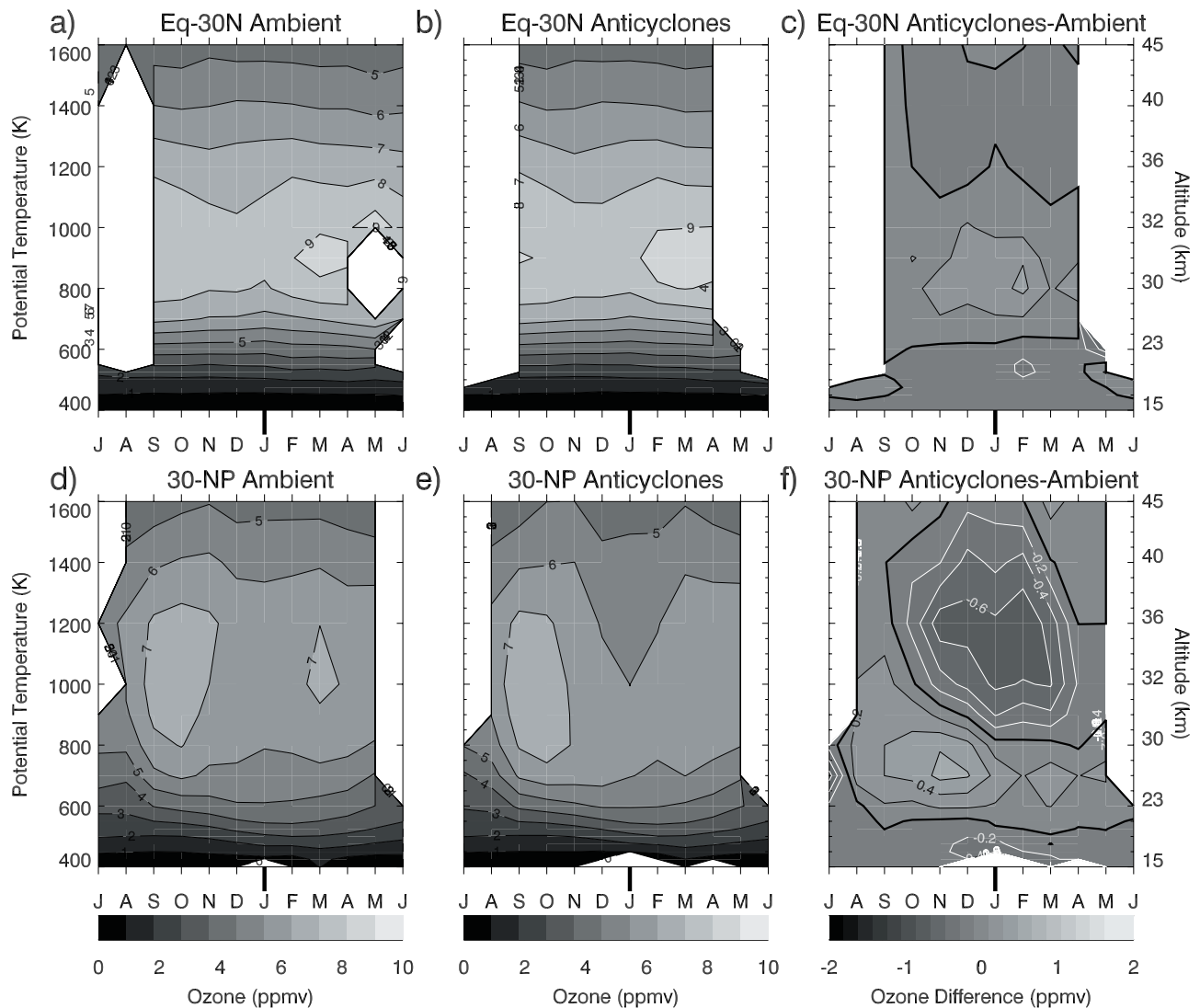


Figure 4. The 12-year composite annual cycle of ozone as a function of altitude in the following Northern Hemisphere air mass types: (a) equator to 30°N ambient, (b) equator to 30°N anticyclones, (c) equator to 30°N anticyclones minus ambient, (d) 30°–90°N ambient, (e) 30°–90°N anticyclones, and (f) 30°–90°N anticyclones minus ambient. The tick mark denoting January is emphasized. Ozone is given in ppbv. In Figures 4c and 4f, differences are given in terms of ppbv (contour interval of 0.2 ppbv). Black (white) contours indicate positive (negative) differences.

full hemispheric mean and has the advantage of being influenced to a lesser degree by anomalies in other air masses (i.e., polar vortices and anticyclones). Aside from chemical sources and sinks, fluctuations in ambient ozone are limited to when anticyclone/vortex air is detrained into ambient regions or when ambient air with differing ozone is entrained into an anticyclone or polar vortex. Monthly mean ozone increases from less than 1 ppbv in the lower stratosphere to more than 9 ppbv near 900 K. Above 900 K, ozone decreases to less than 5 ppbv toward the stratopause. Vertical ozone gradients are twice as large below the ozone maximum as above. From ≈ 700 K to 1200 K, ozone is lowest in winter whereas below ozone is highest in the winter. The distribution of ozone shown here agrees with the climatology of SBUV and SBUV/2 data at 28°N [Randel and Wu, 1995].

[18] Figure 4b shows the 12-year composite annual cycle of ozone in anticyclones between the equator and 30°N as a function of altitude. There is no contribution from POAM or ILAS within this range of latitudes. Note, no anticyclones are identified above 500 K from May through August. Overall, ozone in anticyclones evolves in much the same way as in ambient regions. Figure 4c shows the difference between ozone in anticyclones and in ambient air masses in the equator to 30°N latitude band (Figure 4b minus Figure 4a). Largest differences are found near 800 K in the winter where there is ≈ 0.5 ppbv more ozone in anticyclones compared to ambient regions. While the magnitude of this anomaly is only 5%, it is consistent with tropical ozone being preferentially entrained into subtropical anticyclones compared to ambient regions. The transition to a negative anomaly below 600 K is likewise a result of

enhanced poleward transport into anticyclones (below the ozone maximum, the “geometry” of the ozone distribution is such that ozone is lowest in the tropics).

[19] Figure 4d shows the 12-year composite annual cycle of ozone in ambient air poleward of 30°N. Mean mixing ratios at 1000 K are near 7 ppmv, 2 ppmv lower than at low latitudes. Vertical ozone gradients are also smaller, especially during the winter, because of the increased photochemical lifetime of ozone. These results agree with the SBUV ozone climatology at 60°N [Randel and Wu, 1995]. Figure 4e shows the 12-year composite annual cycle of ozone in anticyclones poleward of 30°N. The SAGE plus HALOE and POAM plus ILAS only climatologies show very similar ozone distributions at higher latitudes. There are clearly differences between ozone in this family of anticyclones and ozone in high-latitude ambient regions (compare to Figure 4d). Figure 4f shows these differences (Figure 4e minus Figure 4d). In the lower stratosphere (below ≈ 600 K), there is up to 0.5 ppmv (50%) less ozone in anticyclones in winter and spring. This is consistent with previous studies that show poleward excursions of subtropical air are collocated with low ozone and anticyclonic ridging in the lower stratosphere [e.g., Orsolini *et al.*, 1995]. This is supported by the fact that only SAGE plus HALOE (lower-latitude samples) contribute to the anomaly.

[20] Between 600 K and 900 K, largest ozone differences occur from September to December where there is up to 1 ppmv (10%) more ozone in anticyclones. This large positive anomaly is observed in both the SAGE plus HALOE and POAM plus ILAS climatologies. It results from the poleward transport of high tropical ozone into anticyclones at this time of year in this altitude range. The altitude and timing of this anomaly suggests that it is to some extent physically connected to the positive anomaly observed at lower latitudes. Above 900 K, there is low ozone in anticyclones. This “LOP regime” is sufficiently sampled and represented in both individual climatologies (SAGE plus HALOE and POAM plus ILAS), with the magnitude of the anomalies being $\approx 10\%$ more pronounced in POAM plus ILAS. The low-ozone anomaly is due to in situ photochemical loss that causes the ozone-rich, anticyclone air to acquire the lower ozone mixing ratios more typical of the equilibrium conditions at the higher latitudes [Morris *et al.*, 1998; Nair *et al.*, 1998]. The largest negative anomaly occurs near 1200 K in February. This is the month of peak LOP probability (shown in section 5).

[21] Near 900 K there is a rapid transition of the ozone anomaly in anticyclones from positive below to negative above. The altitude of this transition approximates the shift in ozone from being dynamically controlled below to photochemically controlled above. This transition altitude between the “LOP regime” and the “Tropical regime” (below) descends from ≈ 1200 to 800 K from September through January. At 900 K there is a positive anomaly in the fall that turns into a negative anomaly by spring. Factors that may contribute to the transition at this altitude include (but are not limited to) anticyclone lifetime, latitude, and degree of isolation. Harvey *et al.* [2002] show that anticyclones in the NH winter do occur more frequently (≈ 12 versus 3%) at 60°N than in fall (see their Figure 6). These high-latitude anticyclones are likely longer lived and more isolated than their fall counterparts but quantitative

estimates of these differences have not been made. To summarize, at high latitudes the relative concentration of ozone in anticyclones compared to ambient regions largely reflects the relative concentrations of O₃ in the tropics and in midlatitudes as a function of altitude. This is the pure transport signal. Superimposed on this signal is the chemical signal, determined by the relative strength of photochemical production (O₂ + hv; O + O₂ + M) and loss (i.e., through the NO_x catalytic cycle).

[22] Figure 5 presents the climatology of ozone in SH anticyclones. Figure 5a shows the 12-year composite annual cycle of ozone in ambient regions between the equator and 30°S as a function of altitude. Ozone peaks in the summer near 900 K and its vertical structure is similar to that observed in the NH. These results, including the slight enhancement in ozone (compared to the NH) during the summer maximum, agree with SBUV ozone at 28°S [Randel and Wu, 1995]. Figure 5b shows the 12-year composite annual cycle for ozone in SH anticyclones between the equator and 30°S. There is no contribution from POAM or ILAS between 30°S and the equator. In addition, no tropical anticyclones are identified above 600 K from November through February. Figure 5c shows the difference between ozone in anticyclones and in ambient air masses in the equator to 30°S latitude band (Figure 5b minus Figure 5a). There is a positive anomaly near 800 K that reaches a maximum (only 2% but still large enough to influence trend calculations) in the spring. As in the NH, it is argued here that this anomaly (as well as the negative anomaly at 500 K) is a result of enhanced poleward transport of tropical air in anticyclones compared to ambient regions.

[23] Figure 5d shows the evolution of ozone in ambient regions poleward of 30°S as a function of altitude. Ozone is near 7 ppmv between 800 and 1200 K, with a 1 ppmv “bite” removed in May and June near 900 K. This results from the higher ozone values being preferentially binned into the anticyclone category. Figure 5e shows the 12-year composite annual cycle of ozone in anticyclones between 30° and 90°S as a function of altitude. As in the NH at 900 K, ozone is enhanced in the fall and diminished in the winter compared to ambient regions. Unfortunately, the POAM plus ILAS instruments do not contribute enough samples in anticyclones to construct a SH climatology. Thus differences shown here solely result from SAGE and HALOE data. Figure 5f illustrates these differences (Figure 5e minus Figure 5d). Below 600 K from May through August, there is ≈ 0.5 ppmv (50%) less ozone in anticyclones than ambient regions. At 800 K, a positive ozone anomaly of about 1 ppmv persists from March through September. This indicates that influx of ozone rich air is dominant over in situ ozone loss at this altitude. From May through October, the negative anomaly between ≈ 900 and 1600 K indicates where and when in situ photochemical ozone loss dominates over in mixing of ozone-rich migrating anticyclones. The jaggedness of this LOP regime is likely due to under sampling.

4. Low-Ozone Pockets

[24] The combined effect of LOPs is to produce the 1200 K negative ozone anomaly in anticyclones shown in the previous section. In this section, we address the LOP contribution to the climatology. LOPs affect the climatology

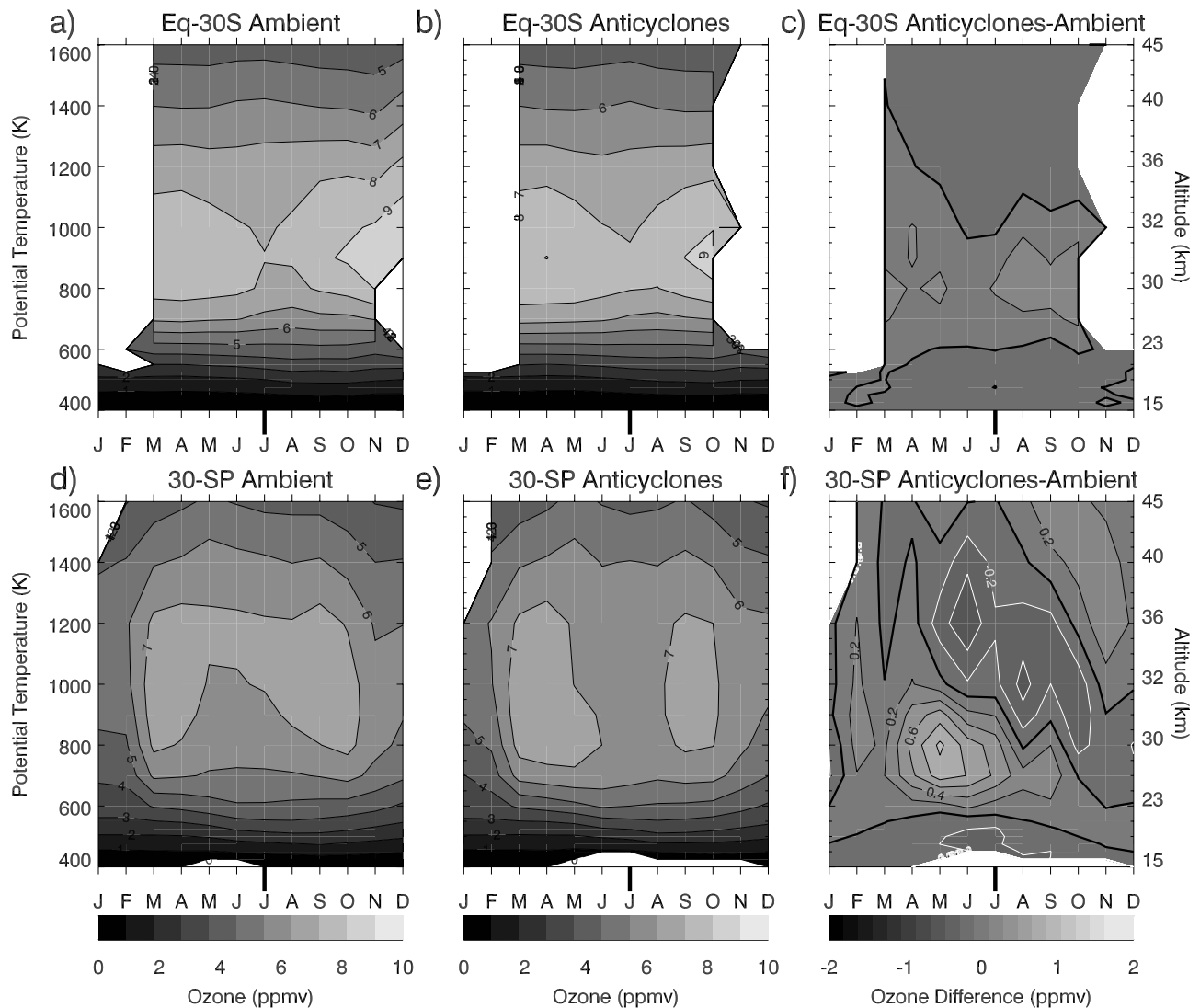


Figure 5. Same as Figure 4 but in the Southern Hemisphere. The time axis is shifted such that the winter season is in the middle of each plot. The July tick mark is emphasized.

of ozone in anticyclones by obscuring the ozone-rich signature in air transported poleward from low latitudes. As mentioned above, this occurs as air sequestered in the anticyclones equilibrates to the lower ozone values appropriate for the high-latitude solar insolation conditions. In this section we present a climatology of the pockets as a means of better quantifying their effects on the anticyclone ozone climatology shown in the previous section.

4.1. Low-Ozone Pocket Catalog

[25] A catalog of LOPs (Appendix A) between November 1991 and November 2003 was generated using data from the solar occultation instruments included in the anticyclone ozone climatology presented in section 3. These LOPs were identified by qualitatively examining the ozone data as a function of longitude, altitude, and time. Anticyclone position was interpolated to each vertical (longitude-altitude) ozone section to indicate the 3-D structure of anticyclones in the vicinity of the ozone measurements. Daily sequences showed the time evolution of ozone in the context of anticyclone life cycles. The case study in this

section shows that during the development of a LOP, high ozone is entrained into the parent anticyclone. Over the course of a few days, providing the anticyclone migrates poleward, a distinct local ozone minimum forms in the anticyclone somewhere between 600 and 1600 K. The ozone minima are conspicuous because of large spatial ozone gradients at the anticyclone edge. Ozone concentrations rapidly increase radially outward from 3 to 6 ppbv in the pocket to values between 7–10 ppbv at the edge. From a longitude-altitude perspective, a pocket is often round or oblate. Variations to this quasi-circular shape depend on the 3-D structure of the intersection between the anticyclone and the ozone measurements. Anticyclones that are upright and do not tilt out of the plane of the ozone measurement area contain pockets that extend into the upper stratosphere. The LOP catalog documents these ozone structures in the occultation data, especially if they persisted and could be tracked for several days moving with the anticyclone.

[26] In Appendix A, 108 pockets are documented and the following information on individual pockets is given: dates

and latitudes detected, approximate altitude range, lifetime, and detecting instrument. There are 60 (48) pockets in the NH (SH). Dates of five LOPs previously documented using UARS Microwave Limb Sounder (MLS) data [Manney *et al.*, 1995c] and nine high ozone surges detected by the Global Ozone Monitoring by Occultation of Stars (GOMOS) instrument between 25 and 40 km over Bern, Switzerland [Calisesi *et al.*, 2001], are incorporated into the catalog. Abbreviations in the catalog represent the following instruments: “G”, GOMOS; “H”, HALOE; “I”, ILAS; “M”, MLS; “P”, POAM; and “S”, SAGE. With the exception of April 1998, high ozone events reported by Calisesi *et al.* [2001] occur in conjunction with a LOP documented here. This is consistent with observations (shown in the next section) of anomalously high ozone just outside of LOP regions; however, the relationship between these two phenomena has not yet been firmly established. The range of latitudes does not necessarily imply poleward movement during the dates detected, although this is often the case. There are cases when one satellite sweeps completely through a pocket (before it dissipates) and then another satellite appears to sweep through it a few days later. When such a temporal gap occurs during the observation of a pocket, it is assumed to be the same pocket if, after closer inspection, the parent anticyclone remained quasi-stationary. A limitation of this catalog is that the dates and latitudes of LOP observations are highly dependent on the limited spatial sampling inherent in occultation measurements. LOP lifetime is estimated given the number of days it was detected. This provides a conservative estimate of the actual lifetime because of incomplete sampling. The LOP that lasted for 49 days is one of only several LOPs sampled over the complete life of the parent anticyclone. Generally speaking, the lifetime of each LOP is directly related to that of its parent anticyclone and will usually be some length less than the life of the anticyclone. The situation is complicated in that pockets do persist after the anticyclone has dissipated. In general, pocket lifetime is proportional to the photochemical lifetime of ozone but also depends on the time it takes to completely mix the pocket into the ambient environment. Quantifying how long LOPs remain after the anticyclone is gone is beyond the scope of this paper.

[27] This catalog is by no means complete and should be regarded as a first attempt toward documenting LOPs. In fact, there are instances when a satellite observes a pocket “suspect” or remnant for 1 or 2 days that are not included in the catalog. Generating a more comprehensive list using data with higher spatial and temporal resolution is a topic for future work.

[28] For each pocket in the catalog, a composite “LOP profile” may be generated from all profiles that intersected the pocket during its life. For the case study shown here, an intersection is assumed for local ozone minima less than 5.5 ppmv between 900 and 1000 K in an anticyclone. The 5.5 ppmv threshold near 900 K is not to be considered a formal LOP definition. It was used for the following case study because it reliably separated the profiles in the anticyclone from those outside. A more general definition (based on spatial gradients perhaps) is needed in future studies. A corresponding mean profile of ambient ozone results from all profiles in ambient regions within 10° latitude of the pocket. Figure 6 shows the composite LOP

profile (black) and ambient profile (grey) for the LOP event during February/March 1999 in the Northern hemisphere (Figure 6a) and September/October 2002 in the Southern hemisphere (Figure 6b). The two pockets were observed at similar latitudes and seasons in each hemisphere. The composite LOP profile for the NH (SH) event resulted from 34 (15) intersecting profiles. Both pockets shown here extend from about 750 to 1400 K. Minimum ozone is found near 1000 K. A characteristic feature of profiles that intersect LOPs is the elevated ozone above and below the pocket. High ozone on either side (east/west) of the pocket is represented by the mean ambient profile.

[29] Figure 7 illustrates some of the information in the catalog. Figure 7a shows the number of LOPs in each hemisphere during each month of the year. Pockets form during months when the polar vortex is present. There are fewer pockets in the SH, but this is likely due to under-sampling. There are anticyclonic disturbances in the SH winter (despite being farther equatorward than in the NH) that likely form LOPs within them (LOPs are observed as far equatorward as 20° and are common near 30°S where anticyclones reside in the winter). SAGE and HALOE simply do not provide enough coverage to fully characterize them. During SH fall and spring anticyclones are prevalent at high latitudes and LOPs within them are common. Unfortunately, they are not sufficiently sampled here. Figure 7b is a probability distribution function of LOP lifetime. Pocket lifetimes range from 3 to 49 days with most LOPs lasting 10 days. This is a conservative estimate since the latitude of the satellite largely determined the start and end dates. Figure 7c shows the distribution of the LOPs in the catalog in latitude and potential temperature. LOPs require the high-latitude conditions under which ozone loss dominates production. Most pockets are observed between 30° and 60° latitude and from 700 to 1200 K in either hemisphere. Since LOPs are confined to anticyclones, it is not surprising that they would occur most often between 30° and 60° latitude [Harvey *et al.*, 2002]. This latitudinal distribution represents a subset of all LOPs and it is likely that, because of the omission of the circumpolar anticyclones and to sampling limitations of the solar occultation, LOPs exist near the pole but were not observed. That LOPs are less prevalent below 700 K stems from the fact that, in the lower stratosphere, the chemical lifetime of ozone is long compared to the time it takes dynamical processes to redistribute it (ozone mixing ratios are conserved during long-range transport). Their decline in the upper stratosphere stems from the fact that ozone’s chemical lifetime is so short that there is no difference between anticyclonic and ambient air. Only in the range of altitudes where dynamical and photochemical lifetimes are of similar magnitudes are the LOPs observed [Morris *et al.*, 1998].

[30] Over the course of surveying the occultation data in search of LOPs the following characteristics were repeatedly observed:

[31] 1. Pockets preferentially develop between 0 and 90°E and dissipate between the date line and 270°E. This longitude preference can be explained to some degree in that anticyclones themselves form and propagate in preferred longitude bands [Harvey *et al.*, 2002].

[32] 2. Pockets follow the movement of their “parent” anticyclone and merge when anticyclones merge. These

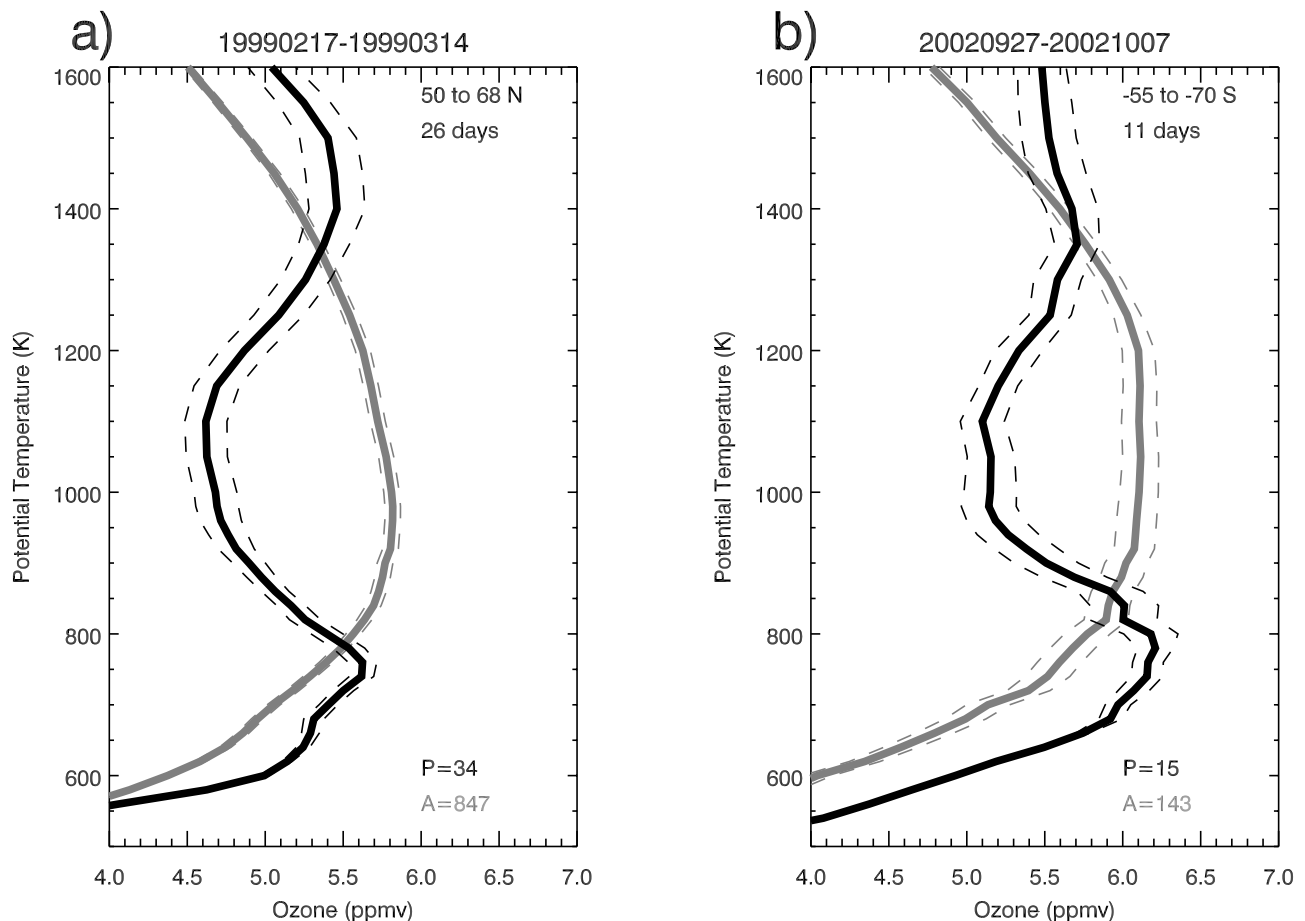


Figure 6. Mean low-ozone pockets (LOP) (black) and ambient (grey) ozone profiles during a LOP event in the (a) Northern Hemisphere and (b) Southern Hemisphere. Dashed lines give estimates of uncertainty (the standard deviation divided by the square root of the number of points). (left) Mean ozone profiles for the February/March 1999 pocket near 60°N. (right) Mean ozone profiles for the September/October 2002 pocket near 60°S. The range of latitudes and pocket lifetime is given in the upper right corner. In the lower right corner the number of profiles intersecting the pocket is indicated by “P=”. The number of ambient profiles is given by “A=.”

merger events are not entirely unexpected but have yet to be documented. Movement of LOPs can be followed continuously for days and weeks at a time.

[33] 3. Pockets form without an anticyclone at all or in ridges with very small regions of recirculation. This suggests minimal isolation is required for LOP development. These pockets are short-lived and are not included in the catalog.

[34] 4. Pockets reach higher altitudes at higher latitudes. This observation is consistent with the photochemical lifetime of O₃ increasing with increasing latitude.

[35] 5. Pockets descend from the upper to the middle stratosphere over their lifetimes. Pockets establish rapidly in the upper stratosphere where photochemical lifetimes are short. This coupled with wintertime descent may account for the apparent downward movement of LOPs.

4.2. Low-Ozone Pocket Case Study

[36] In this section, the evolution of a LOP that formed in the NH in December of 1993 is shown from the point of view of the observing satellites. This particular pocket was chosen from the family of 108 because it is partic-

ularly well defined and has been previously observed in MLS data [Manney *et al.*, 1995c; Morris *et al.*, 1998; Nair *et al.*, 1998]. The reader is referred to these studies for detailed analyses of the surrounding meteorological conditions, air parcel motions, and photochemistry associated with the development of this and several other LOPs. Figures 8a–8d include snapshots of the LOP on 26 November, 29 November, 3 December, and 10 December 1993, respectively. On these select days during the life of the pocket, polar projections at 1000 K (top row) illustrate how the shape of the polar vortex changes, the location of anticyclones, and the position of satellite measurements relative to these dynamical structures. In each polar plot, the Arctic vortex is over the pole and a satellite is measuring ozone inside the Aleutian High at different stages of the anticyclone’s development. These ozone slices capture the structure and evolution of the pocket in the zonal, vertical, and in so far as the satellite is sweeping north-south in time, the meridional directions. In these altitude sections, the thick black (white) contour depicts the vortex (anticyclone) edge at the latitude of the satellite. The thin horizontal white line at 1000 K indicates the

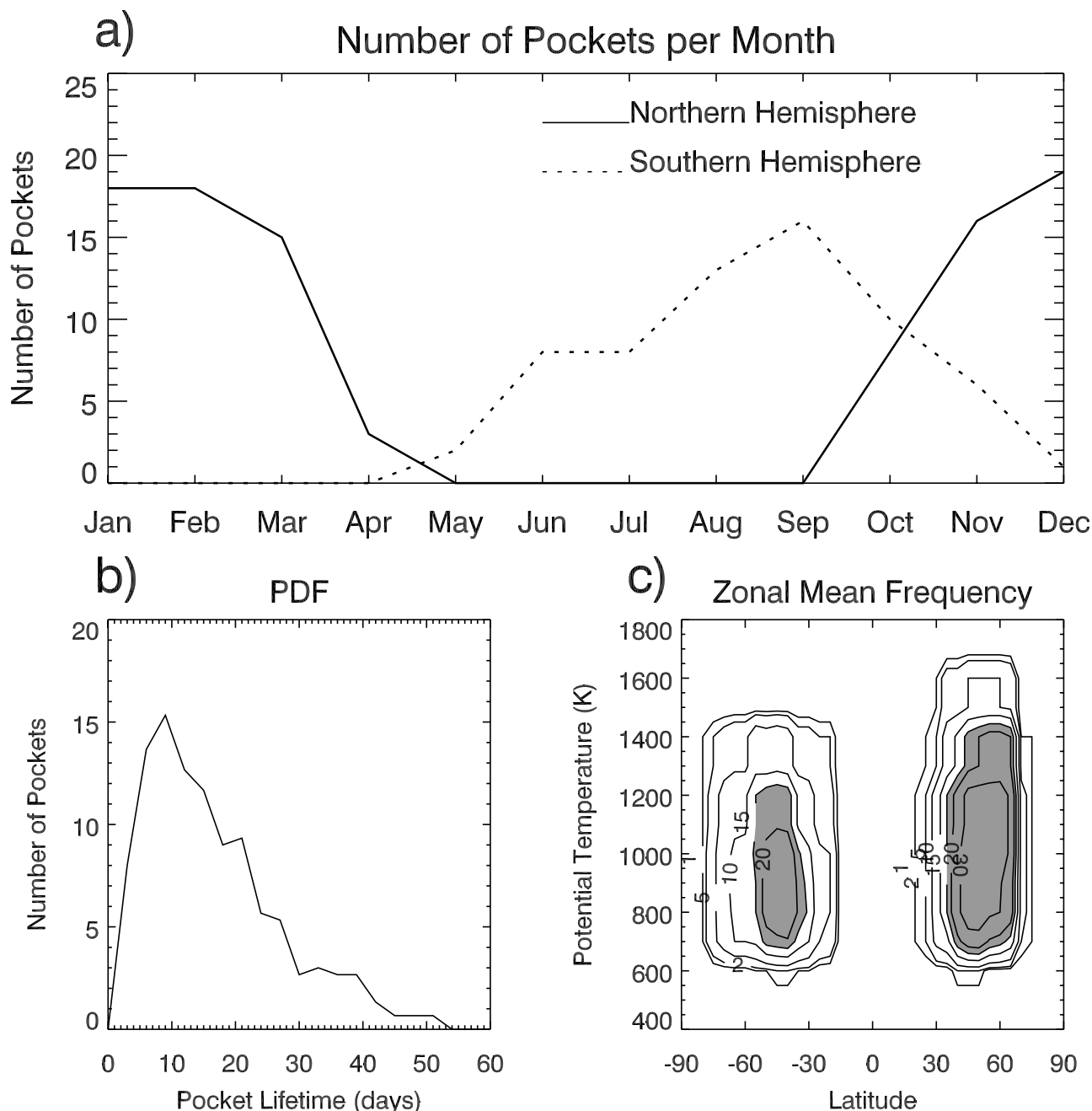


Figure 7. Statistics from the LOP catalog. (a) Total number of LOPs per month over the 1991–2003 time period. The solid (dotted) line is for LOPs in the Northern (Southern) Hemisphere. (b) Probability distribution function of LOP lifetime. (c) Number of pockets as a function of latitude and altitude. Contours are irregularly spaced. Regions with more than 15 pockets are shaded.

altitude of the polar plot. The bottom row shows the individual ozone profiles on each day. Red (blue) symbols are superimposed on profiles located in the anticyclone (Arctic vortex). The geographical location of these ozone profiles is shown in the polar projections in the top row.

[37] On 26 November (Figure 8a) the polar projection shows the Arctic vortex over the pole and the Aleutian High off the east coast of Asia, where it formed 2 days earlier. HALOE measurements are located along the poleward flank of the anticyclone on this day. The longitude-altitude section below it shows both the zonal

and vertical structure of the anticyclone and the ozone field at $\approx 50^\circ\text{N}$ latitude. The anticyclone (white contour) is located near 150°E , extends from ≈ 600 to 1200 K, and tilts slightly westward with height adjacent to the vortex (black contour). We infer the transport of a deep layer of tropical air into the anticyclone by the high mixing ratios (8 – 9 ppmv) present inside the anticyclone at 50°N from 700 K to 1200 K (a layer 10 – 15 km deep). The ozone profiles (bottom row) show ozone mixing ratios in the anticyclone are near 8 ppmv compared to 6 ppmv at other longitudes. This is consistent with previous studies that

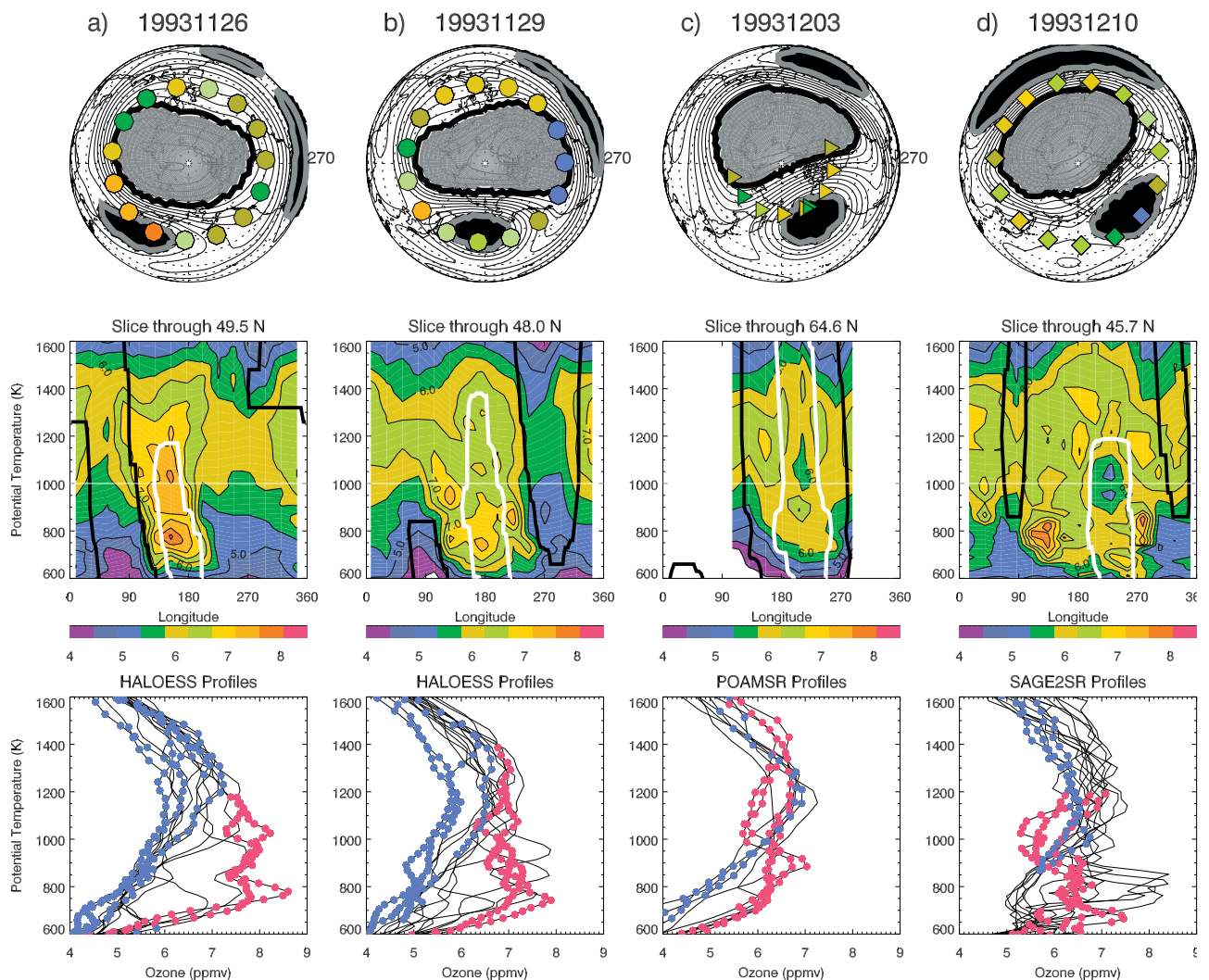


Figure 8. (top) Polar projections at 1000 K, (middle) longitude-altitude ozone sections at the latitude of the satellite, and (bottom) individual ozone profiles for (a) 26 November, (b) 29 November, (c) 3 December, and (d) 10 December 1993. In the top row the Arctic vortex is grey with a black edge; anticyclones are black with a grey edge. The stream function field is contoured (contour interval is 2.5×10^{-7}). Satellite measurement locations are colored according to ozone mixing ratio. The 270°E longitude points to the right. The date line is oriented toward the bottom such that this longitude matches up with the center of the longitude-altitude ozone sections in the middle row. In the middle row the thick black (white) contour depicts the vortex (anticyclone) edge at the latitude of the satellite. The thin horizontal white line at 1000 K indicates the altitude of the polar plot. In the bottom row, red (blue) symbols are superimposed on profiles located in the anticyclone (Arctic vortex).

show tropical air transported poleward between the vortex and an anticyclone and subsequently being entrained into the anticyclone [e.g., Manney *et al.*, 1995b; Waugh, 1996; Riese *et al.*, 2002].

[38] The first indication of the LOP occurred 2 days later (28 November) as HALOE swept equatorward and sampled in the core of the anticyclone. Manney *et al.* [1995c] also show this LOP beginning to form on this day and, since MLS collected data in the NH for several days before that, this verifies that it was indeed just forming. In general, incorporating ozone data with higher spatial sampling is needed for a more precise determination of the time of LOP formation and decay. Figure 8b shows the vortex, anticyclone, and ozone field on 29 November (when the pocket was slightly more developed). The polar

projection shows an elongated Arctic vortex and the Aleutian High over the date line. HALOE measurements now sample the equatorward flank of the anticyclone. The longitude-altitude section shows the anticyclone reaches higher altitudes (1400 K) and ozone inside the anticyclone has decreased at all levels. The LOP is in the anticyclone near 1100 K. There are three ozone profiles in the anticyclone with mean values near 7 ppmv.

[39] On 3 December (Figure 8c) the polar projection shows the Aleutian High continued to amplify and move slowly eastward. The anticyclone also moved poleward such that POAM II sampled the LOP near 65°N latitude. The longitude-altitude section shows the anticyclone extends through the depth of the stratosphere on this day. The LOP is located in the anticyclone between

Table A1. Low-Ozone Pocket Catalog

Start-End Dates ^a	N Latitudes	Altitudes	Life, days	Instrument ^b
19911129–19920103	31°–48°	800–1400 K	36	H, S
19920106–19920126	40°–50°	700–1200 K	21	H, S
19920209–19920229	45°–52°	800–1200 K	21	H, S
19920322–19920416	60°–70°	700–1200 K	26	H, S
19921001–19921020	45°–65°	700–1400 K	20	S
19921028–19921206	40°–50°	700–1000 K	40	H, S
19921208–19930104	30°–48°	700–1200 K	28	H, S
19921212–19921224	40°–48°	10–5 hPa	28	M
19930124–19930222	40°–53°	700–1400 K	30	H, S
19930225–19930314	52°–61°	800–1200 K	18	S
19930223–19930307	67°–70°	10–5 hPa	18	M
19931014–19931019	45°–55°	700–900 K	6	S
19931025–19931114	50°–55°	700–1400 K	21	H, S
19931128–19931221	33°–48°	800–1200 K	24	H, S
19931128–19931218	59°–62°	10–5 hPa	24	M
19931223–19940122	46°–49°	700–1400 K	31	H, S
19940122–19940201	40°–52°	600–1000 K	11	H
19940201–19940226	39°–57°	700–1400 K	26	H, S
19940305–19940320	54°–59°	700–1400 K	16	H, S
19940327–19940418	60°–75°	700–1400 K	23	H, S
19941030–19941110	40°–54°	700–1000 K	12	H, S
19941110	47°	25–40 km	12	G
19941112–19941123	47°	700–1000 K	12	H
19941122–19941128	47°	25–40 km	12	G
19941124–19941205	26°–48°	700–1200 K	12	H, S
19941227–19950203	37°–50°	800–1200 K	39	H, S
19950321–19950329	55°–65°	700–1400 K	9	H, S
19951102–19951119	45°–67°	1000–1400 K	18	H, S, P
19960106–19960204	37°–66°	700–1400 K	30	H, S, P
19960203–19960209	47°	25–40 km	30	G
19960215–19960304	47°–67°	700–1200 K	19	H, S, P
19960310–19960311	47°	25–40 km	9	G
19960309–19960317	57°–68°	1000–1400 K	9	H, S, P
19960318–19960322	57°–62°	1000–1400 K	5	H, S, P
19961028–19961109	42°–70°	800–1200 K	13	H, S, P, I
19961118–19961123	66°–68°	700–1000 K	6	I
19961214–19970131	25°–65°	700–1400 K	49	H, S, I
19961225–19961230	47°	25–40 km	49	G
19970203–19970211	36°–53°	600–800 K	9	S
19970212–19970226	40°–55°	700–1200 K	15	H, S
19970312–19970326	40°–60°	900–1200 K	15	H, S
19971113–19971230	40°–50°	700–1000 K	48	H, S
19971226–19971229	47°	25–40 km	48	G
19980116–19980123	47°	25–40 km	19	G
19980128–19980215	35°–54°	700–1200 K	19	S
19980226–19980305	47°	25–40 km	7	G
19980304–19980310	57°–61°	700–1200 K	7	H, S
19980320–19980325	45°–67°	800–1200 K	6	H
19980411–19980418	47°	25–40 km	6	G
19981012–19981025	41°–60°	700–1200 K	14	H, S, P
19981106–19981122	45°–68°	800–1200 K	17	H, P
19981204–19981211	63°–65°	800–1200 K	8	H, S, P
19990129–19990215	43°–67°	800–1400 K	18	H, S, P
19990217–19990314	50°–68°	1000–1400 K	26	H, S, P
19991127–19991205	47°–65°	800–1400 K	9	H, S, P
19991211–19991220	33°–64°	800–1200 K	10	H, S, P
19991226–20000130	30°–66°	700–1200 K	36	H, S
20000201–20000212	47°–67°	700–1400 K	12	S, P
20000309–20000401	43°–68°	700–1400 K	24	H, S, P
20001112–20001201	40°–66°	800–1400 K	20	H, S, P
20001205–20001217	35°–65°	800–1600 K	13	H, S, P
20001213–20010105	18°–64°	700–1200 K	24	H, P
20010115–20010215	35°–65°	800–1600 K	32	H, S, P
20011024–20011027	30°–42°	700–1200 K	4	H
20011130–20020107	30°–64°	800–1600 K	39	H, P
20020110–20020127	35°–66°	800–1400 K	18	S, P
20020209–20020303	43°–67°	700–1600 K	23	H, S, P
20021126–20021203	42°–65°	700–1200 K	8	H, S, P
20021208–20030112	35°–64°	700–1400 K	36	H, P
20030119–20030207	45°–65°	1000–1600 K	20	H, S, P
20030211–20030226	54°–68°	700–1400 K	16	H, P

Table A1. (continued)

Start-End Dates	S Latitudes	Altitudes	Life	Instrument ^b
19920625–19920802	30°–50°	700–1000 K	39	H, S
19920824–19920901	35°–50°	800–1200 K	9	S
19920912–19920919	40°–55°	900–1400 K	8	H, S
19920928–19921028	45°–70°	700–1400 K	31	H, S
19930716–19930729	39°–49°	800–1200 K	14	H, S
19930813–19930826	32°–47°	800–1000 K	14	H, S
19930822	44°–46°	10 hPa	14	M
19930929–19931006	50°–65°	700–1200 K	8	H, S
19931104–19931117	60°–75°	700–1000 K	14	S, P
19940530	50°–58°	10 hPa	9	M
19940602–19940610	40°–46°	600–900 K	9	H, S
19940713–19940717	40°–50°	700–1000 K	5	H, S
19940718–19940728	20°–45°	700–1000 K	11	H, S
19940804–19940821	30°–50°	700–900 K	18	H, S
19940823–19940826	30°–55°	600–800 K	4	S
19940906–19940909	40°–55°	1000–1400 K	4	H, S
19940910–19940920	40°–55°	800–1400 K	11	H, S
19941007–19941020	40°–65°	700–900 K	14	H
19941030–19941206	55°–75°	700–1400 K	38	S, P
19950618–19950621	30°–40°	700–900 K	4	S
19950816–19950827	47°–56°	700–1200 K	12	S
19950913–19950919	62°–65°	900–1400 K	7	H, S
19951009–19951026	57°–62°	700–1200 K	18	H
19951108–19951124	63°–72°	700–1200 K	17	H, S, P
19960624–19960718	28°–45°	700–1400 K	25	H, S
19960715–19960802	30°–45°	800–1200 K	19	H, S
19960807–19960815	40°–53°	800–1400 K	9	S
19960911–19960920	55°–62°	700–1400 K	10	H, S
19960921–19960927	40°–64°	800–1200 K	7	H, S
19961031–19961102	65°–75°	700–1200 K	3	S, P
19961113–19961127	60°–70°	700–1200 K	15	P, I
19970520–19970524	25°–40°	700–1000 K	5	H, S
19970609–19970626	20°–40°	800–1400 K	18	H, S
19970726–19970731	20°–35°	700–1400 K	6	H, S
19970802–19970823	40°–55°	700–1400 K	22	H, S
19970822–19970831	38°–53°	700–1200 K	10	S
19970915–19970921	45°–60°	1000–1400 K	7	H, S
19980621–19980629	20–50°	700–1200 K	9	H, S
19990904–19990911	35°–45°	700–1000 K	8	H, S
19991009–19991015	40°–58°	700–1200 K	7	S
20000823–20000902	33°–52°	700–1200 K	11	H
20000907–20000913	58°–60°	700–1000 K	7	H
20001020–20001114	65°–80°	700–1400 K	26	H, P
20010828–20010906	47°–50°	700–900 K	10	H, S
20020513–20020601	27°–50°	800–1200 K	20	H, S
20020609–20020705	20°–50°	700–1000 K	27	H, S
20020820–20020831	30°–55°	800–1200 K	12	H, S
20020927–20021007	55°–70°	800–1200 K	11	S
20030902–20030930	35°–66°	700–1000 K	29	H, S

^aFormat is year/month/day.

^bInstrument definitions are as follows: G, GOMOS; H, HALOE; I, ILAS; M, MLS; P, POAM; and S, SAGE.

≈1000 K and 1200 K where ozone levels are less than ≈6 ppmv. Two of the nine profiles sampled the pocket and are easily distinguished from the other profiles at 1100 K. At this altitude, mean ozone levels in the pocket are less than 6 ppmv compared to 6.5–7 ppmv outside the pocket.

[40] A week later on 10 December (Figure 8d) the polar plot shows the Aleutian High continued to move eastward and is located off the west coast of North America. SAGE II measurements sample ozone in the anticyclone near 46°N latitude. The longitude-altitude slice indicates a well defined pocket of low ozone between 900 K and 1100 K in the anticyclone. The anticyclone does not extend as high at this latitude because it tilts back across the pole (not shown). By this time, ozone mixing ratios in the pocket approach 5 ppmv. High ozone observed on either side and above and below the pocket denotes regions receiving a continuous

supply of tropical air. On either side of the pocket (especially visible at 800 K) the ozone maxima represent air recently in the tropics that is flowing between the anticyclone and the vortex. The ozone profiles indicate a clear separation of air masses in the 900–1100 K layer with ozone mixing ratios in the pocket approaching 5 ppmv compared to 6–7 ppmv outside. The pocket appears to descend with time, which result from sampling the pocket at different latitudes (the pocket is not expected to be spherical, but extend to higher altitudes farther poleward).

[41] Both the entrainment of high ozone into anticyclones and the subsequent development of LOPs within them occurs repeatedly each winter. The ozone climatology presented in the previous section showed the net effect of binning both very high and very low ozone values together in anticyclones. This implies that there is more ozone

variability in anticyclones than in the rest of the atmosphere. This could be used to argue for the removal of ozone data in anticyclonic air masses when calculating ozone trends.

5. Summary and Discussion

[42] In this study, the distribution of stratospheric ozone is examined as a function of air mass type. Satellite ozone measurements taken in anticyclones and in polar vortices are separated from those corresponding to ambient regions. This paper quantifies the net distribution of ozone in anticyclones, and compares this to ambient ozone.

[43] Both dynamical and chemical processes control the distribution of ozone in anticyclones in the middle stratosphere. The relative importance of dynamics and chemistry depends on latitude, altitude, and season. This study was motivated by repeatedly observing air masses rich in ozone moving poleward and being entrained into developing anticyclones. The goal of this work was to determine whether these events, that occur on synoptic timescales, result in a signature of high ozone in anticyclones in a climatological sense. Results indicate that they do. However, it was realized that the formation of LOPs in stratospheric anticyclones, a chemical process, is often just as important in determining ozone levels in anticyclones and needs to be considered hand in hand with dynamics for a complete understanding. Because of this, an inventory of LOPs observed between 1991 and 2003 by the satellites used here is provided. The dates, latitudes, and approximate altitude ranges of 108 pockets are included. This catalog provides the most comprehensive documentation on LOPs to date and aids in the interpretation of climatological ozone anomalies in anticyclones.

[44] Results of the ozone climatology are presented as a function of altitude, hemisphere, and season. Since the photochemical lifetime of ozone increases dramatically with latitude, results are computed for two latitude groups divided at 30°. During summer in both hemispheres, dynamical structures are weak and ozone gradients between different air mass types are small. However, during fall, winter, and spring the following ozone differences are observed. In the lower winter stratosphere, there is ≈ 0.5 ppmv (30%) less ozone in anticyclones compared to ambient regions. This is consistent with earlier work where subtropical air with low ozone was found coincident with anticyclonic ridging in the lower stratosphere [Orsolini et al., 1995]. Between 600 and 1000 K both high- and low-latitude anticyclones are associated with elevated ozone. The low-latitude anomaly in the NH (SH) is largest (2–5%) in February (October). At high latitudes, the NH (SH) positive anomaly maximizes (10%) in November (May). This is likely due to the entrainment of tropical ozone into low-latitude anticyclones and their subsequent poleward migration. In both hemispheres, the magnitude of this positive ozone anomaly wanes into spring as a result of LOP formation. Near 900 K there is a rapid transition of the ozone anomaly in anticyclones from positive below to negative above. The altitude of this transition approximates the shift in ozone from being dynamically controlled below to photochemically controlled above. Above this altitude, the formation of LOPs within anticyclonic circulation systems results in 10% less ozone in anticyclones than ambient regions. These anomalies are

sufficiently large to argue for the removal of ozone data in anticyclonic air masses (and thus some natural atmospheric variability) when calculating ozone trends.

[45] There are 60 (48) pockets in the NH (SH) observed by the occultation instruments used in this study. LOPs form during months when the polar vortex is present. There are fewer pockets in the SH, but this is likely due to under-sampling. Pocket lifetimes range from 3 to 49 days with most LOPs lasting 10 days. This is a conservative estimate since the latitude of the satellite largely determined the start and end dates. LOPs require the high-latitude conditions under which ozone loss dominates production. Most pockets are observed between 30° and 60° latitude and from 700 to 1200 K in either hemisphere. Future work will examine inter-annual variability and trends in the climatology and in LOPs.

Appendix A

[46] Table A1 documents low-ozone pockets observed by one or more of the satellite occultation instruments used in this study. Pocket dates range from November 1991 through September 2003. Northern and Southern Hemisphere pockets are listed separately.

[47] **Acknowledgments.** We would like to thank colleagues at the Met Office for producing the stratospheric assimilated data set. We are grateful to the British Atmospheric Data Centre for providing us with access to the MetO data. For data processing and distribution we thank those involved with the HALOE, SAGE II, POAM and ILAS science teams. The POAM instruments are sponsored by the Office of Naval Research with contributions from the NASA data purchase program. The ILAS project is supported by the Ministry of the Environment of Japan. We thank the reviewers for their insightful comments which improved the quality of this manuscript. Support for this work was provided by the NASA Atmospheric Chemistry Modeling and Analysis Program. M.H.H. was funded by NASA grant NAG-1-2162.

References

- Abrams, M. C., et al. (1996), ATMOS/ATLAS-3 observations of long-lived tracers and descent in the Antarctic vortex in November 1994, *Geophys. Res. Lett.*, *23*, 2341–2344.
- Calisei, Y., H. Wernli, and N. Kampfer (2001), Midstratospheric ozone variability over Bern related to planetary wave activity during the winters 1994–1995 to 1998–1999, *J. Geophys. Res.*, *106*, 7903–7916.
- Chen, P., J. R. Holton, A. O'Neill, and R. Swinbank (1994), Isentropic mass exchange between the tropics and extratropics in the stratosphere, *J. Atmos. Sci.*, *51*, 3006–3018.
- Choi, W., S. Kim, W. B. Grant, M. Shiotani, Y. Sasano, and M. R. Schoeberl (2002), Transport of methane in the stratosphere associated with the breakdown of the Antarctic polar vortex, *J. Geophys. Res.*, *107*(D24), 8209, doi:10.1029/2001JD000644.
- Cunnold, D. M., L. Froidevaux, J. M. Russell, B. Connor, and A. Roche (1996), Overview of UARS ozone validation based primarily on intercomparisons among UARS and Stratospheric Aerosol and Gas Experiment II measurements, *J. Geophys. Res.*, *101*, 10,335–10,350.
- Douglass, A. R., and R. B. Rood (1986), Derivation of photochemical information near 1 mbar from ozone and temperature data, *J. Geophys. Res.*, *91*, 13,153–13,156.
- Fairlie, T. D. A. (1995), Three-dimensional transport simulations of the dispersal of volcanic aerosol from Mount Pinatubo, *Q. J. R. Meteorol. Soc.*, *121*, 1943–1980.
- Finger, F. G., R. M. Nagatani, M. E. Gelman, C. S. Long, and A. J. White (1995), Consistency between variations of ozone and temperature in the stratosphere, *Geophys. Res. Lett.*, *22*, 3477–3480.
- Garcia, R. R., and S. Solomon (1985), The effect of breaking gravity waves on the dynamics and chemical composition of the mesosphere and lower thermosphere, *J. Geophys. Res.*, *90*, 3850–3868.
- Gettelman, A., and P. M. de Forster (2002), Definition and climatology of the tropical tropopause layer, *J. Meteorol. Soc. Jpn.*, *80*, 911–924.
- Grant, W. B., E. V. Browell, C. S. Long, L. L. Stowe, R. G. Grainger, and A. Lambert (1996), Use of volcanic aerosols to study the tropical stratospheric reservoir, *J. Geophys. Res.*, *101*, 3973–3988.

- Harvey, V. L., M. H. Hitchman, R. B. Pierce, and T. D. Fairlie (1999), Tropical aerosol in the Aleutian High, *J. Geophys. Res.*, *104*, 6281–6290.
- Harvey, V. L., R. B. Pierce, and M. H. Hitchman (2002), A climatology of stratospheric polar vortices and anticyclones, *J. Geophys. Res.*, *107*(D20), 4442, doi:10.1029/2001JD001471.
- Haynes, P. H. (1990), High-resolution three-dimensional modeling of stratospheric flows: Quasi-two-dimensional turbulence dominated by a single vortex, in *Topological Fluid Mechanics*, edited by H. K. Moffat and A. Tsinover, pp. 345–354, Cambridge Univ. Press, New York.
- Hitchman, M. H., M. McKay, and C. R. Trepte (1994), A climatology of stratospheric aerosol, *J. Geophys. Res.*, *99*, 20,689–20,700.
- Kent, G. S., C. R. Trepte, U. O. Farrukh, and M. P. McCormick (1985), Variation in the stratospheric aerosol associated with the north cyclonic polar vortex as measured by the SAM II satellite sensor, *J. Atmos. Sci.*, *42*, 1536–1551.
- Kreher, K., G. E. Bodeker, H. Kanzawa, H. Nakane, and Y. Sasano (1999), Ozone and temperature profiles measured above Kiruna inside, at the edge of, and outside the Arctic polar vortex in February and March 1997, *Geophys. Res. Lett.*, *26*, 715–718.
- Kulikov, Y. Y., A. A. Krasil'nikov, and V. G. Ryskin (2002), Microwave studies of the structure of the polar-latitude ozone layer during winter anomalous warming events in the stratosphere, *Atmos. Oceanic Phys.*, *38*, 158–166.
- Lahoz, W. A., et al. (1993), Northern Hemisphere mid-stratosphere vortex processes diagnosed from H₂O, N₂O and potential vorticity, *Geophys. Res. Lett.*, *20*, 2671–2674.
- Lahoz, W. A., et al. (1994), Three-dimensional evolution of water vapor distributions in the Northern Hemisphere stratosphere as observed by the MLS, *J. Atmos. Sci.*, *51*, 2914–2930.
- Lahoz, W. A., et al. (1996), Vortex dynamics and the evolution of water vapour in the stratosphere of the Southern Hemisphere, *Q. J. R. Meteorol. Soc.*, *122*, 423–450.
- Lary, D. J. (1997), Catalytic destruction of stratospheric ozone, *J. Geophys. Res.*, *102*, 21,515–21,526.
- Leovy, C. B., et al. (1985), Transport of ozone in the middle stratosphere: Evidence for planetary wave breaking, *J. Atmos. Sci.*, *42*, 230–244.
- Lorenz, A. C., et al. (2000), The Met. Office Global three-dimensional variational data assimilation scheme, *Q. J. R. Meteorol. Soc.*, *126*, 2992–3012.
- Malvern, L. E. (1969), *Introduction to the Mechanics of a Continuous Medium*, 713 pp., Prentice-Hall, Old Tappan, N. J.
- Manney, G. L., L. Froidevaux, J. W. Waters, L. Elson, E. F. Fishbein, R. W. Zurek, R. S. Harwood, and W. A. Lahoz (1993), The evolution of ozone observed by UARS MSL in the 1992 late winter southern polar vortex, *Geophys. Res. Lett.*, *20*, 1279–1282.
- Manney, G. L., et al. (1995a), Lagrangian transport calculations using UARS data. Part I: Passive tracers, *J. Atmos. Sci.*, *52*, 3069–3081.
- Manney, G. L., et al. (1995b), Lagrangian transport calculations using UARS data. Part II: Ozone, *J. Atmos. Sci.*, *52*, 3069–3081.
- Manney, G. L., L. Froidevaux, J. W. Waters, R. W. Zurek, J. C. Gille, J. B. Kumer, J. L. Mergenthaler, A. E. Roche, A. O'Neill, and R. Swinbank (1995c), Formation of low-ozone pockets in the middle stratospheric anticyclone during winter, *J. Geophys. Res.*, *100*, 13,939–13,950.
- Manney, G. L., et al. (1998), The 4-day wave and transport of UARS tracers in the Austral polar vortex, *J. Atmos. Sci.*, *55*, 3456–3470.
- Manney, G. L., H. A. Michelsen, F. W. Irion, G. C. Toon, M. R. Gunson, and A. E. Roche (2000), Lamination and polar vortex development in fall from ATMOS long-lived trace gases observed during November 1994, *J. Geophys. Res.*, *105*, 29,023–29,038.
- Manney, G. L., III, G. C. Toon, and J. M. Zawodny (2001), Comparison of satellite ozone observations in coincident air masses in early November 1994, *J. Geophys. Res.*, *106*, 9923–9943.
- Michelsen, H. A., G. L. Manney, M. R. Gunson, and R. Zander (1998), Correlations of stratospheric abundances of NO_y, O₃, N₂O, and CH₄ derived from ATMOS measurements, *J. Geophys. Res.*, *103*, 28,347–28,359.
- Michelsen, H. A., et al. (1999), Intercomparison of ATMOS, SAGE II, and ER-2 observations in Arctic vortex and extra-vortex air masses during spring 1993, *Geophys. Res. Lett.*, *26*, 291–294.
- Morris, G. A., S. R. Kawa, A. R. Douglass, and M. R. Schoeberl (1998), Low-ozone pockets explained, *J. Geophys. Res.*, *103*, 3599–3610.
- Morris, G. A., J. F. Gleason, J. M. Russell III, M. R. Schoeberl, and M. P. McCormick (2002), A comparison of HALOE V19 with SAGE II V6.00 ozone observations using trajectory mapping, *J. Geophys. Res.*, *107*(D13), 4177, doi:10.1029/2001JD000847.
- Nair, H., M. Allen, L. Froidevaux, and R. W. Zurek (1998), Localized rapid ozone loss in the northern winter stratosphere: An analysis of UARS observations, *J. Geophys. Res.*, *103*, 1555–1571.
- Newman, P. A., et al. (1996), Measurements of polar vortex air in the midlatitudes, *J. Geophys. Res.*, *101*, 12,879–12,891.
- O'Neill, A., et al. (1994), Evolution of the stratosphere during northern winter 1991/92 as diagnosed from U. K. Meteorological Office analyses, *J. Atmos. Sci.*, *51*, 2800–2817.
- Orsolini, Y., D. Cariolle, and M. Deque (1995), Ridge formation in the lower stratosphere and its influence on ozone transport: A general circulation model study during late January 1992, *J. Geophys. Res.*, *100*, 11,113–11,135.
- Perliski, L. M., and J. London (1989), Satellite observed long-term averaged seasonal and spatial ozone variations in the stratosphere, *Planet. Space Sci.*, *37*, 1509–1525.
- Pierce, R. B., et al. (1994), Evolution of Southern Hemisphere spring air masses observed by HALOE, *Geophys. Res. Lett.*, *21*, 213–216.
- Plumb, R. A. (2002), Stratospheric transport, *J. Meteorol. Soc. Jpn.*, *80*, 793–809.
- Polvani, L. M., D. W. Waugh, and R. A. Plumb (1995), On the subtropical edge of the stratospheric surf zone, *J. Atmos. Sci.*, *52*, 1288–1309.
- Proffitt, M. H., et al. (1989), A chemical definition of the boundary of the Antarctic ozone hole, *J. Geophys. Res.*, *94*, 11,437–11,448.
- Randall, C. E., et al. (1995), Preliminary results from POAM II: Stratospheric ozone at high northern latitudes, *Geophys. Res. Lett.*, *22*, 2733–2736.
- Randall, C. E., et al. (2003), Validation of POAM III ozone: Comparisons with ozonesonde and satellite data, *J. Geophys. Res.*, *108*(D12), 4367, doi:10.1029/2002JD002944.
- Randel, W. J., and F. Wu (1995), Climatology of stratospheric ozone based on SBUV and SBUV/2 data: 1978–1994, *NCAR Tech. Note TN-412+STR*, Natl. Cent. for Atmos. Res., Boulder, Colo.
- Randel, W. J., et al. (1993), Stratospheric transport from the tropics to middle latitudes by planetary wave mixing, *Nature*, *365*, 533–535.
- Rasch, P. J., B. A. Boville, and G. P. Brasseur (1995), A three-dimensional general circulation model with coupled chemistry for the middle atmosphere, *J. Geophys. Res.*, *100*, 9041–9071.
- Riese, M., G. L. Manney, J. Oberheide, X. Tie, R. Spang, and V. Kull (2002), Stratospheric transport by planetary wave mixing as observed during CRISTA-2, *J. Geophys. Res.*, *107*(D23), 8179, doi:10.1029/2001JD000629.
- Rood, R. B., A. Douglass, and C. Weaver (1992), Tracer exchange between tropics and middle latitudes, *Geophys. Res. Lett.*, *19*, 805–808.
- Rusch, D. W., et al. (1997), Validation of POAM ozone measurements with coincident MLS, HALOE, and SAGE II observations, *J. Geophys. Res.*, *102*, 23,615–23,627.
- Ruth, S. L., J. J. Remedios, B. N. Lawrence, and F. W. Taylor (1994), Measurements of N₂O by the UARS Improved Stratospheric and Mesospheric Sounder during the early northern winter 1991/92, *J. Atmos. Sci.*, *51*, 2818–2833.
- Seo, K.-H., and K. P. Bowman (2000), Levy flights and anomalous diffusion in the stratosphere, *J. Geophys. Res.*, *105*, 12,295–12,302.
- Sugita, T., et al. (2002), Validation of ozone measurements from the Improved Limb Atmospheric Spectrometer, *J. Geophys. Res.*, *107*(D24), 8212, doi:10.1029/2001JD000602.
- Swinbank, R., and A. O'Neill (1994), A stratosphere-troposphere data assimilation system, *Mon. Weather Rev.*, *122*, 686–702.
- Trepte, C. R., and M. H. Hitchman (1992), Tropical stratospheric circulation deduced from satellite aerosol data, *Nature*, *355*, 626–628.
- Trepte, C. R., R. E. Veiga, and M. P. McCormick (1993), The poleward dispersal of Mount Pinatubo volcanic aerosol, *J. Geophys. Res.*, *98*, 18,563–18,575.
- Ward, W. E., J. Oberheide, M. Riese, P. Preusse, and D. Offermann (2000), Planetary wave two signatures in CRISTA 2 ozone and temperature data, in *Atmospheric Science Across the Stratopause*, *Geophys. Monogr. Ser.*, vol. 123, edited by D. E. Siskind, S. D. Eckermann, and M. E. Summers, pp. 319–325, AGU, Washington, D. C.
- Waugh, D. W. (1993), Subtropical stratospheric mixing linked to disturbances in the polar vortices, *Nature*, *365*, 535–537.
- Waugh, D. W. (1996), Seasonal variation of isentropic transport out of the tropical stratosphere, *J. Geophys. Res.*, *101*, 4007–4023.
- Waugh, D. W. (1997), Elliptical diagnostics of stratospheric polar vortices, *Q. J. R. Meteorol. Soc.*, *123*, 1725–1748.
- Yang, H. (1995), Three-dimensional transport of the Ertel potential vorticity and N₂O in the GFDL SKYHI model, *J. Atmos. Sci.*, *52*, 1513–1528.

T. D. Fairlie and R. B. Pierce, NASA Langley Research Center, Hampton, VA 23681-0001, USA.

V. L. Harvey and C. E. Randall, Laboratory for Atmospheric and Space Physics, University of Colorado, Boulder, CO 80309-0392, USA. (harvey@aura.colorado.edu)

M. H. Hitchman, Department of Atmospheric and Oceanic Sciences, University of Wisconsin, Madison, WI 53706, USA.